www.elsevier.com/locate/bios

Synthesis and application of a "plastic antibody" in electrochemical microfluidic platform for oxytocin determination

Piyush Sindhu Sharma, Zofia Iskierko, Krzysztof Noworyta, Maciej Cieplak, Pawel Borowicz, Wojciech Lisowski, Francis D'Souza, Wlodzimierz Kutner

PII: S0956-5663(17)30616-4
DOI: http://dx.doi.org/10.1016/j.bios.2017.09.009
Reference: BIOS9983

To appear in: *Biosensors and Bioelectronic*

Received date: 6 June 2017
Revised date: 13 August 2017
Accepted date: 7 September 2017

Cite this article as: Piyush Sindhu Sharma, Zofia Iskierko, Krzysztof Noworyta, Maciej Cieplak, Pawel Borowicz, Wojciech Lisowski, Francis D'Souza and Wlodzimierz Kutner, Synthesis and application of a "plastic antibody" in electrochemical microfluidic platform for oxytocin determination, *Biosensors and Bioelectronic,* http://dx.doi.org/10.1016/j.bios.2017.09.009

Synthesis and application of a "plastic antibody" in electrochemical microfluidic platform for oxytocin determination

Piyush Sindhu Sharma,[a,*] Zofia Iskierko,[a] Krzysztof Noworyta,[a] Maciej Cieplak,[a] Pawel Borowicz,[a]

Wojciech Lisowski,[a] Francis D'Souza[b] and Wlodzimierz Kutner [a,c]

[a]Institute of Physical Chemistry, Polish Academy of Sciences,

Kasprzaka 44/52, 01-224 Warsaw, Poland

[b]Department of Chemistry, University of North Texas, Denton, 1155,

Union Circle, #305070 TX 76203-5017, USA

[c]Faculty of Mathematics and Natural Sciences, School of Sciences,

Cardinal Stefan Wyszynski University in Warsaw, Wóycickiego 1/3, 01-815 Warsaw, Poland

Corresponding Author *E-mail: psharma@ichf.edu.pl

Abstract

By means of molecular imprinting of a conducting polymer, molecular cavities selective for oxytocin nonapeptide, an autism biomarker, were designed. Embedding of the oxytocin template and then its extracting from the molecularly imprinted polymer (MIP) was confirmed by the XPS analysis. AFM imaging of the MIP film surface indicated changes in mechanical properties of the film after template extraction. The MIP synthetic receptor was deposited by potentiodynamic electropolymerization as a thin film on an Au film electrode in an electrochemical miniaturized microfluidic cell. The use of this cell allowed to shorten analysis time and to decrease the sample volume. The linear dynamic concentration range extended from 0.06 to 1 mM with the limit of detection of 60 μM (S/N=3). Advantageously, sensitivity of the diagnostic microfluidic platform devised for oxytocin determination in both synthetic serum samples and in aqueous solutions was similar, and moreover it was selective to common interferences, such as oxytocin analogs and potential metabolites.

Keywords

Plastic antibody, Electroactive functional monomer, Microfluidics, Autism biomarker, Oxytocin.

Introduction

Autism is a neurological disorder of the brain. It affects the ability of the child to communicate, relate, and socialize. Children with autism often reveal repetitive behaviors or body movements and do not like any changes in the daily routine (Anderson 2015; Frustaci et al. 2012). These symptoms usually develop before the age of three (Yates and Couteur 2008). Autism is now recognized as a group of syndromes denoted as the autism spectrum disorder (ASD). The prevalence of ASD is currently estimated to be 6-7 per 1000, affecting 4 times more boys than girls. Unfortunately, the present diagnosis of ASD can reliably be made only by the age of three, because the core symptoms emerge not until that time. Therefore, determination of ASD at an early stage at the age before three is in demand.

Mass spectrometry (MS) is a versatile tool used for investigation of endogenous protein changes. It can be useful to identify the possible ASD biomarkers, whose determination in blood, saliva or urine can help in ASD diagnosing (Woods et al. 2013). Other samples which can be used for analysis of this disorder include brain tissues and the cerebrospinal fluid. However, sample collection in this case is difficult, painful, and cannot be performed in every laboratory. Several factors can affect the MS analysis of these samples on each step, i.e., sample preparation, data analysis, and data interpretation. Although one MS experiment can produce an enormous amount of information, the data analysis limits this method, because it needs involvement of an expert (Woods et al. 2013).

Various studies showed that an oxytocin nonapeptide hormone (Green et al. 2001; Modahl et al. 1998) concentration level in body fluids in patients with diagnosed ASD is different than that in healthy individuals. Therefore, oxytocin can be used as a biomarker for autism. Moreover, there is an increasing interest in measuring peripheral oxytocin levels to better understand the role of this peptide in mammalian behavior, physiology, and diseases.

Until now, concentration of oxytocin has been measured by enzyme- and radioimmunoassay in body fluids, such as blood plasma, saliva, and urine as well as in the cerebrospinal fluid (Szeto et al. 2011). The obtained results suggested pretreatment of samples. Importantly, further analysis showed the presence of multiple immunoreactive products interfering with oxytocin in sample extracts, which casts doubts on reliability of these assays. An increasing interest in the role of oxytocin in mammals proves that there is a critical need to establish valid and reliable procedures to determine this peptide in body fluids (Szeto et al. 2011).

Other than immunoassays approach, label free method, such as HPLC with UV detection have been used toward oxytocin determination in biological samples. However, most of these methods required time-consuming sample preparation procedures, such as protein precipitation, solvent extraction, and

solid-phase extraction to concentrate oxytocin in plasma (Kukucka and Misra 1994; Mabrouk and Kennedy 2012; Zhang et al. 2011)

An emerging alternative approach suggests the use of a "plastic antibody" as the replacement for traditional biological receptors in sensing (Haupt and Mosbach 1998). The number of designs and syntheses of biomimetic receptor systems capable of binding target molecules with affinity and selectivity similar to those of natural receptors is rapidly growing (Sharma et al. 2015; Sharma et al. 2012). Importantly, these materials are used as recognition units for devising selective chemical sensors. Molecularly imprinted polymers (MIPs) (Sharma et al. 2013) represent an excellent example of synthetic systems that mimic recognition encountered in animate nature. These "smart materials" can selectively and reversibly bind only the target analyte because of the presence of dedicated imprinted molecular cavities in the polymer structure. Several reports described the previous attempts of imprinting of oxytocin (Lin et al. 2006; Rachkov and Minoura 2000; Yola et al. 2015; Zheng et al. 2007). These attempts resulted in devising solid-phase extraction materials for oxytocin separation (Lin et al. 2006; Rachkov and Minoura 2000).

Electrochemical detection systems based on microchip platforms are recently becoming popular for implementing field-portable devices because of high sensitivity, possibility of miniaturization and the ease of use (Birnbaumer et al. 2009; Hong et al. 2010 ; Weng et al. 2007). These easy-to-use and sensitive analytical tools are necessary for detecting very low concentrations of the target analyte of the health care importance (Weng et al. 2007).

Towards attaining this goal, we deposited in the present work the devised MIP synthetic receptor in the form of a thin film on a commercial Au disk thin-film electrode surface. Then, this MIP coated Au electrode was assembled in an electrochemical microcell to construct a microfluidic platform. Capacitive impedimetry was applied to determine oxytocin molecule binding by dedicated molecular cavities of the MIP synthetic receptor (Ertürk and Mattiasson 2017). The present work proposes an easy and effective way of MIP film preparation and its use as the recognition unit in a microfluidic based impedimetric sensing device.

2. Experimental

2.1 Reagents

Electrochemical grade acetonitrile was purchased from Sigma-Aldrich. Tetrabutylphosphonium tetrafluoroborate, (TBP)BF_4, was from Fluka. Synthetic details on preparation of the 4-*bis*(2,2'-bithien-5-yl)methylbenzoic acid glycol ester **FM 1** functional monomer is given in Supporting Information. Synthetic details on other functional monomers including 1-methylamide-4-[*bis*(2,2'-

bithienyl)methane **FM 2** (Huynh et al. 2013), and *bis*(2,2'-bithienyl)-(4-(2-hydroxyethoxy)phenyl)methane **FM 3** (Huynh et al. 2015a), as well as the 2,4,5,2',4',5'-hexa(thiophen-2-yl)-3,3'-bithiophene **CM** (Sannicolò et al. 2016) cross-linking monomer are given elsewhere. All the synthesized monomers were purified by HPLC before use. Analytical grade NaOH and KF were procured from CHEMPUR.

2.2. Instrumentation and procedures

Structure of the pre-polymerization complex was optimized in vacuum and in a solvent by computational modeling using the density functional theory (DFT) at the B3LYP level with the 3-21G* basis set, all implemented in the Gaussian 09 software package (Frisch *et. al.* 2009).

XPS spectra were recorded on a PHI 5000 VersaProbe™ (ULVC-PHI) scanning ESCA microprobe using monochromatic A1 Kα radiation ($h\nu$=1486.4 eV). The XPS data were generated by a 100-μm diameter X-ray beam and collected from 250-μm^2 irradiated area. High-resolution XPS spectra were collected with a hemispherical analyzer at the pass energy of 23.5 eV, energy step of 0.1 eV, and photoelectron take off angle of 45° with respect to the surface plane. CASA XPS software was used to evaluate the XPS data. The background was subtracted using the Shirley method and peaks were fitted using the mixed Gaussian-Lorentzain method. The binding energy of the Au 4f7/2 peak (*BE* = 84.0 eV) was chosen as an internal reference.

Infrared (IR) spectra were recorded with a Vertex 80v Fourier Transform IR (FTIR) computer controlled Bruker spectrometer equipped with Opus 6.5 software of the same manufacturers. In order to measure an IR signal from thin polymer films, a PMA50 module was used. This module enables carrying out polarization-modulation infrared reflection-absorption spectroscopy (PM IRRAS) measurements. Spectra were recorded with 2-cm^{-1} resolution. For each spectrum, 1024 scans were recorded. The experimental IR spectra were compared with those theoretically generated. Theoretical vibration frequencies of normal modes were calculated with the DFT method within harmonic approximation. Positions of the bands in experimental spectra were determined with the procedure implemented in the Opus 6.5 software package. Calculated normal modes were assigned to experimental bands in two-steps. The first vibrational energy distribution analysis (VEDA) step calculated normal modes expressed in terms of local modes (vibrations of internal coordinates: bonds, i.e., bond angles, and dihedral angles) (Jamróz 2004-2010, 2013). In the second step, the spectra calculated were fitted to experimental data by means of linear regression. That way, the unharmonic factor was phenomenologically introduced to calculated frequencies. Those calculated frequencies were scaled with the SPESCA program (Jamróz 2014).

AFM topography and nanomechanical property images were recorded using Multimode 8 microscope of Bruker equipped with a Nanoscope V controller operating in the PeakForce QNM mode. Nanoscope v.8.15 software was used for data acquisition and analysis. An RTESP silicon tip on the silicon cantilever with the spring constant of 42 Nm^{-1} was used for all experiments. The reduced Young modulus was calculated from the force curves recorded using the DMT model. For determining average film thickness, some parts of the film were carefully removed in few different places from the electrode surface, i.e., scratched with a Teflon™ spatula, under an optical microscope. Subsequently, these scratches were imaged with AFM. Then, heights of the resulting steps were measured by averaging the number of points on both sides of the step (sufficiently far from its partially detached front). The difference of the average values of points on the step and at its foot determined the height of the step. Finally, step heights measured for different scratches were averaged to get an average value of film thickness.

The electropolymerization under potentiodynamic conditions and capacitance measurements were performed using an SP-300 BioLogic potentiostat controlled by EC-Lab BioLogic software.

Polymer samples for XPS, IR, and AFM measurements were deposited on glass slides coated with thin layers of Au evaporated on Ti underlayers (Au-glass slides).

Au thin-film electrodes were purchased from MicruX Technologies. Before measurements, electrodes were electrochemically activated by potential cycling 25 times in 0.5 M H_2SO_4 between 0 and 1.30 V at the rate of 50 mVs^{-1}. The working (1-mm diameter), reference, and counter electrodes were made from Au and fabricated by a thin-film technology. For deposition of MIP films on Au electrodes, the external Ag/AgCl reference electrode and the Pt wire counter electrode were used in a three-electrode one-compartment V-shaped electrochemical glass mini cell.

All MIP films were deposited by potentiodynamic electropolymerization. Pre-polymerization solution contained the oxytocin template, **FM 1**, and **CM**, at the molar ratio of 1 : 4 : 2. The presence of the cross-linking monomer incurred three-dimensionality to the MIP matrix. Moreover, the solution was 0.1 M in tetrabutylphosphonium tetrafluoroborate, which served as the supporting electrolyte. Finally, five potential cycles at the 50 mVs^{-1} scan rate were performed to complete the MIP film deposition. After deposition, the film was rinsed with abundant acetonitrile to remove excess of the supporting electrolyte and non-polymerized monomers. Then, the oxytocin template was extracted from the MIP film by holding at constant potential of 0.50 V vs. Ag/AgCl applied to the MIP film coated electrode in 0.01 M NaOH for 8 h. To confirm the imprinting, a control polymer (non-imprinted polymer, NIP) was prepared in the absence of oxytocin.

A commercial microfluidic system (MicruX Technologies) was used for the capacitance measurement under flow-injection analysis (FIA) conditions. This system was composed of the aluminum base

and the methacrylate cover (Scheme 1). A wall-jet flow-through electrochemical microcell featured a standard microfluidic port with the inlet channel of 0.5 mm in I.D. The internal volume of the cell was <500 nL. The cell volume was limited by the O-ring (2- or 3- mm I.D.). The frequency and potential applied to the MIP film coated working electrode was kept constant at f =20 Hz and E_{appl}=0.50 V, respectively. The microfluidic system was connected to a programmable syringe pump Model 78/100 of KD Scientific allowing controlling the flow rate of 35 μL min^{-1}. A 10 mM KF was used as the carrier solution all throughout the measurements.

Scheme 1

3. Result and discussion

3.1 Molecular cavity designing in the imprinted polymer

Bioreceptors offer specific interaction with the target analyte. Notably, the specificity of bioreceptors is incurred by their molecular cavities, in which different recognition sites are positioned in a well-defined manner to provide definite chemical microenvironment for reversible binding of target analyte molecules. For instance, these cavities in protein bioreceptors are generated by arrangement of a series of amino acids joined by peptide bonds in a polypeptide chain. Therefore, to mimic these microcavities in MIPs, artificial multi-point interacting monomers should be designed. Molecules of these monomers should be able to self-assemble around the template molecule, similarly as amino acid molecules in protein receptors.

Accordingly, we have designed and synthesized a few functional monomers (Scheme 2) non-covalently binding the oxytocin template through multiple-point interactions. These monomers contained the bisbithiophene polymerizable moiety. The presence of this moiety allowed “freezing”, by electropolymerization, the arrangement of functional monomer molecules around the template molecule. Before final application of the functional monomers for the imprinting, structures of the pre-polymerization complexes of the oxytocin template and selected functional monomers were optimized by computational modeling.

Scheme 2

The change in Gibbs free energy (ΔG) of formation of the oxytocin complexes with different functional monomers were calculated with the density functional theory (DFT) method. Firstly, 1 : 1 com-

plex formation was allowed to be formed. The calculated ΔG values of different pre-polymerization 1 : 1 complexes are summarized in Table S1. The negative gain of ΔG was the highest for the complex of oxytocin with **FM 1** (Table S1). This ΔG value was the most negative if this ratio was 1 : 4 (Scheme S1 and Table S1). However, further increase of this ratio resulted in the decrease in the negative ΔG value, possibly because of steric hindrance and overcrowding. Further, the acetonitrile solvent molecules were introduced to study the medium effect on the complexation. Importantly, this complexation in acetonitrile was still possible. With this preliminary screening step, the optimal molar ratio of the template to functional monomer leading to a stable pre-polymerization complex was selected.

3.2 Deposition of the electroactive imprinted polymer film

The solution of optimized composition for electropolymerization contained the oxytocin template, the functional monomer **FM 1**, and the cross-linking monomer **CM** in the molar ratio of 1 : 4 : 2, which followed from the DFT molecular modeling. Then, the structure of this prepared pre-polymerization complex was "frozen" with potentiodynamic electropolymerization resulting in deposition of a synthetic receptor in the form of a thin MIP film on the Au electrode (Fig. S1). An anodic peak appeared at ~1.10 V vs. Ag/AgCl corresponding to irreversible electro-oxidation of the bisbithiophene moieties of the monomers (Huynh et al. 2015b). During this electro-oxidation, cation radicals are formed (Heinze et al. 2010). These radicals initiate electrochemical polymerization, which herein resulted in precipitation of the MIP film on the electrode surface. The anodic peak increased in consecutive cycles indicating formation of a highly conducting MIP film. After completion of the electropolymerization, the supporting electrolyte and unreacted substrates were removed from the MIP film with excess of the acetonitrile solvent.

3.3 Confirmation of oxytocin templating in MIP, and then template removal

A complete template removal from the structurally well-defined MIP molecular cavities is one of the most important steps in MIP preparation for analytical applications. If not, the template may "bleed" from the MIP during analyte determination thus contributing to positive false results. Therefore, confirmation of complete template removal is essential. The population of molecular cavities imprinted in MIP usually correlates with the sensitivity of the devised chemosensor. Therefore, the progress of oxytocin template removal was carefully controlled.

3.3.1 XPS confirmation of template removal from polymer film

For template removal confirmation, high-resolution XPS spectra were recorded in the energy region of nitrogen binding at different stages of template removal (Figure 1) (Yoshimi et al. 2013). Moreover, several buffers and solvents were tested for this removal. Only potentiostatic conditions (0.50 V vs. Ag/AgCl) appeared effective in this removal. Oxytocin templating, and then its removal was manifested by the presence and absence, respectively, of the N 1s peak at ~400 eV in the XPS spectra of the MIP film. The spectrum for the MIP film before template removal clearly confirmed the presence of the N 1s peak (Curve *1* in Figure 1). Eventually, this peak disappeared after template extraction under potentiostatic conditions for at least 8 h in 0.01 M NaOH (curves *2* and *3* in Figure 1). However, a residual N 1s peak was still seen even after 8-h extraction, and it did not decrease even after further extraction. Advantageously, XPS directly confirmed the entrapment, and then removal of oxytocin from the MIP film because the N element was absent in both the functional and cross-linking monomer.

Figure 1

3.3.2 Infrared spectroscopy confirmation of template removal from polymer film

PM IRRAS measurements on the MIP and NIP films were performed to confirm the template presence, and then its absence after removal. Figure S2 shows experimental spectra recorded for the MIP and NIP films before and after potentiostatic template extraction along with the calculated and scaled theoretical frequencies of normal modes. Briefly, the oxytocin-entrapped MIP film showed (Fig. S2a) bands at ~1654, 1704, and 1771 cm^{-1} corresponding to the C=O vibrations of different amide bonds of oxytocin. These bands disappeared after oxytocin extraction (Fig. S2b). The band at ~1722 cm^{-1} corresponds to vibration of the carboxyl group of **FM 1**. Moreover, the band of OH-bending vibration of the tyrosine amino acid moiety of oxytocin was present at ~1380 cm^{-1} (Fig. S2a). Expectedly, intensity of this band was lower for the NIP film (Fig. S2c). More importantly, intensity of this band decreased after oxytocin template extraction (Fig. S2b). Interestingly, a new broad band appeared between 1550–1700 cm^{-1} in the spectrum of the MIP film after extraction, possibly because of generation of the C=O group over the thiophene skeleton because of MIP electrochemical overoxidation.

3.4 Morphology and mechanical properties of the oxytocin imprinted polymer film

We used AFM for direct determination of three-dimensional morphology of conductive MIP and NIP films. Moreover, we used PeakForce QNM mapping to evaluate nanomechanical properties of the deposited and oxytocin-extracted MIP and NIP films.

The determined morphology parameters of the MIP and NIP films before and after oxytocin template extraction are summarized in Table S2. Apparently, the as prepared MIP (Figure 2a) and NIP (Figure 2b) films were relatively thin and rough. Both were composed of rough spherical grains of a hundred nm in diameter. Interestingly, thickness of both MIP and NIP films increased after oxytocin template extraction, most likely because of film swelling (Table S2). Worth mentioning, MIP roughness substantially increased after template extraction because of appearance of many larger grains (Figure 2c). However, NIP film roughness decreased after similar treatment mainly because of the appearance of uniformly distributed larger grains (Figure 2d).

Figure 2

Nanomechanical properties of the films are addressed in Figure 2e-2h, while average values of mechanical parameters characteristic for the films are presented in Table 1. In general, the determined energy dissipation (Figure 2e-2h) corroborated that films were composed of relatively rigid grains connected by softer boundaries. Interestingly, the average energy dissipation markedly increased for both films after extraction (Table 1); this increase was much more pronounced for the MIP than the NIP film. That is, this value was markedly higher (~20 times) for the MIP film after oxytocin template extraction, which indicated softening of the film (Table 1). Interestingly, the dissipation change in the NIP film, after similar treatment, increased merely by ~7 fold. This effect indicates that films became softer and/or adhesion of the polymer to the AFM tip was stronger. Indeed, the average value of the reduced Young modulus decreased for both MIP and NIP films after extraction, pointing out film softening. The decrease of the Young modulus was, again, much more pronounced for the MIP than NIP film. Besides, adhesion force between the tip and the polymer sample increased after extraction for the NIP film but slightly decreased for the MIP film. Noteworthy, values of the reduced Young modulus evaluated herein for all studied films are in the range of modulus (3.5-12 GPa) characteristic for the poly(3-thiophenemethyl acetate) thin films (Madrigal et al. 2013).

Table 1

3.6 Oxytocin determination with an electrochemical microfluidic platform

Typically, a relatively large solution volume is needed to perform an electrochemical experiment under stagnant solution conditions. At a sufficiently high concentration of a supporting electrolyte, diffusion is the only way of mass transport of a redox analyte. But electrochemical measurements performed un-

der controlled flow conditions at the electrode of a smaller area and the cell volume minimized down to the microscale bring significant advantages. Combining controlled convection with diffusion increases the transport rate of the analyte to the electrode surface, thus allowing determination of analytes at lower concentrations. Usually, this convection is introduced to the system by using a solution flow or rotating the electrode. Importantly, this relative solution-electrode movement should precisely be controlled and well defined. Advantageously, the signal-to-noise ratio increases and the sample volume substantially decreases for measurements under flow conditions (Channon et al. 2016).

Therefore, we have measured impedance of the MIP and NIP films under flow-injection analysis (FIA) conditions using this micro cell. These measurements were performed at the direct current potential offset of 0.50 V and the alternating current potential amplitude of 10 mV. During measurements, the frequency was kept constant at f = 20 Hz. At this low frequency, the MIP film-coated electrode mainly reveals capacitive properties (Cheng et al. 2001). This capacitance was low at low potential and it rapidly increased with the potential increase (Mermilliod et al. 1986). However, the capacitance was low again when the polymer was completely oxidized. Therefore, the potential of 0.50 V was selected as an optimized potential in these measurements as no electrochemical process of the polymer occurred in this potential region (Fig. S1).

Moreover, we recorded impedance spectra of MIP film in order to confirm best frequency range for determination of capacitance of MIP film. Corresponding phase angle vs. logarithm of frequency curves are shown in Fig. S3. The plot showed appreciable changes in phase angle of the MIP in low frequency range. Phase angle of the oxytocin templated MIP film was initially ~-43° (curve *1* in Fig S3), which subsequently decreased to ~-58° after oxytocin template extraction (curve *2* in Fig S3). Moreover, the phase angle of oxytocin extracted MIP film increased again after binding with different amounts of oxytocin (curves *3-7*, Fig S3). This increase was most prominent in the low frequency range. Interestingly, impedance spectra indicated that removal of the template from MIP leads to appearance of two electrochemical processes with different time constants, while non-extracted MIP features only one such process. This suggested that impedance spectrum of non-extracted MIP film (curve *1,* Fig. S3) is dominated by bulk polymer parameters at high-frequencies, while for extracted MIP film interfacial effects at low frequencies plays important role (curves *2-7* in Fig S3).

At this constant and sufficiently low frequency, the capacitance of the double layer at the electrode-solution interface can readily be determined (Orazem and Tribollet 2008). This was the case in the present study where the analyte binding strongly affected electric permittivity of this layer. In order to increase sensitivity of this capacitance transduction, the double layer should be relatively thick. Too thin double layer compromises the chemosensor sensitivity by leaving a major analyte portion outside.

When considering this effect, we herein applied a relatively low concentration of a supporting electrolyte (0.01 M KF), which was used as the carrier solution.

After sufficient equilibrating the MIP film coated Au electrode in the carrier solution, oxytocin samples of different concentrations were consecutively injected to the carrier solution at the constant flow rate. As soon as the oxytocin reached the electrode, the electrode-solution interfacial capacitance decreased because of oxytocin molecule interaction with molecular cavities in MIP. This capacitance decrease was reversible. That is, the capacitance increased to its former background value when the oxytocin was eluted with excess of the carrier solution. The determined capacitance was lower (i.e., electric permittivity of the double layer was lower) the higher was the concentration of oxytocin in the consecutively injected samples (Fig. 3a). The linear dynamic concentration range extended from at least 0.06 to 1.0 mM oxytocin with the calibration plot obeying the linear regression equation of *Capacitance*/nF = -1.065(±0.039) $c_{oxytocin}$/mM + 0.0425(±0.020)/nF. The correlation coefficient was 0.997 while the LOD and sensitivity at the signal-to-noise ratio (S/N) of 3 was 60 µM and -1.065(±0.039) nF mM^{-1}, respectively.

To confirm the imprinting, i.e., the presence of selective molecular cavities in the MIP film, two additional experiments were performed. In one, a control non-imprinted polymer (NIP) film was deposited on the Au film electrode under the conditions same as those for MIP except of the oxytocin template absence. When this NIP film was used for capacitance measurements to determine oxytocin under the same conditions, results were quite different than those for MIP. Apparently, oxytocin binding by the NIP was much weaker (Fig. 3b) than that by the MIP film. The calibration plot followed the linear regression equation, *Capacitance*/nF =-0.048(±0.005)$c_{oxytocin}$/mM + 0.002(±0.002)/nF. Evidently, a low NIP film sensitivity to oxytocin confirmed oxytocin imprinting in MIP. From the ratio of the sensitivity of the MIP chemosensor and that of the NIP to oxytocin, the apparent imprinting factor was determined to be as high as, IF = 22. An imprinting factor is the measure of the strength of interaction of the MIP imprinted cavities with the template molecules. That is, the higher the imprinting factor, the stronger the imprinted cavity interacts with the template molecule.

Figure 3

In another experiment, the effect of interferences on the response of the oxytocin-templated MIP capacitive chemosensor was examined. Compounds with similar structure or consisting parts of the oxytocin nonapeptide were chosen as interferences. Even sensitivity to carbetocin, a close oxytocin analog, was low (Fig. 3c). More importantly, biomolecules of a smaller size than that of oxytocin failed

to show any response (Fig. S4). Apparently, highly selective molecular cavities were imprinted in the MIP film.

As demonstrated above, the selection of the appropriate functional monomers for generation of selective molecular cavities in the MIP is crucial for successful imprinting. Now, several approaches toward the selection of the most appropriate monomers are available including the computational modeling explored in the present research. The role of the **CM** is to secure in space the recognizing sites of functional monomers in pre-defined locations and orientation around template molecules and thereby to maintain the structure of the imprinted cavity in the MIP network. Therefore, the use of a proper template-to-**FM 1**-to-**CM** ratio is important for MIP preparation. Herein, it was demonstrated that sensitivity of the MIP film, prepared with a relatively higher CM ratio (template : **FM 1** : **CM** = 1 : 4 : 6) was lower (Fig. S5) in comparison to that of the MIP film prepared with a relatively lower concentration of the cross-linker monomer (template : **FM 1** : **CM** = 1 : 4 : 2) (Fig. 3a). Therefore, the latter ratio was used in subsequent studies.

After finding suitability of the devised microfluidics platform to determine oxytocin in an aqueous solution and optimization of the determination conditions, the system was applied for determination of oxytocin in a synthetic serum sample. For that, a commercial NORTROL serum was diluted 1000 times with the carrier solution. This control serum was prepared from human serum. It contained both human and non-human enzymes as well as the non-protein components. Different concentrations of oxytocin were prepared in control serum samples to examine analytical performance of the chemosensor in this complex matrix. Although the signal recorded for a given concentration of oxytocin was ~20% higher than that for the KF solution of oxytocin, the sensitivity of the chemosensor was nearly the same. The calibration plot was described by the linear regression equation of *Capacitance*/nF = -1.01(±0.05) c_{oxytocin}/mM - 0.48(±0.03) and the correlation coefficient was 0.988 (Fig. 3d). A high signal obtained for the NORTROL control serum samples, compared to that for an aqueous solution, might arise from the presence of small ions in NORTROL leading to different composition of the electrical double layer. Moreover, the similar sensitivity obtained in both aqueous (KF) and in NORTROL control serum sample suggested a high resistance towards protein fouling. A recent report presented result of MIP based synthetic receptor for PSA protein determination in blood plasma (Tamboli et al. 2016). In this case, signals for each protein concentration in buffer and in the plasma sample were different because of the matrix effect. However, this chemosensor was able to determine protein in the plasma sample. Herein, we observed a very similar behavior. Interestingly, our chemosensor was able to determine oxytocin in diluted synthetic serum samples (Fig. 3d). Moreover, the calibration curve, constructed in the same concentration range as that used for an aqueous oxytocin solution, was similar. As mentioned in the Introduction,

various reports described results of oxytocin imprinting (Rachkov and Minoura 2000; Yola et al. 2015; Zheng et al. 2007). However, only few presented the application of the imprinting strategy for fabrication of chemosensor for oxytocin determination in real samples, such as milk (Yola et al. 2015). Therefore, the present report can be considered as the first application of designing molecular cavities by application of electropolymerizable functional monomer for oxytocin determination. Additionally, electropolymerizable functional monomers allowed to deposit MIP, as a thin film, directly on transducer surface, which is much simpler in comparison to commonly used procedure of MIP deposition for devising capacitance chemosensors (Ertürk et al. 2014; Ertürk et al. 2016; Graniczkowska et al. 2017). Moreover, results obtained confirmed applicability of the devised microfluidic platform for oxytocin determination in real samples.

We confirmed reproducibility of devised chemosensor by determining the response signal for the 0.25 mM oxytocin using three different MIP films (Fig. S6). The response signal obtained from these chemosensors was very similar with average value of -0.30 nF. The standard deviation of signal was ±0.02 nF.

4. Conclusions

We successfully combined a microfluidics platform, molecular imprinting, and electrochemical transduction to devise a miniaturized chemosensor for oxytocin determination in biological samples. Selective molecular cavities were carefully generated in a conducting MIP film. For that, suitable functional monomers were selected by computational modeling. With functional monomers multipoint-interacting with the template, it was possible to prepare a pre-polymerization complex stable in both vacuum and the acetonitrile solvent. This complex was transferred successfully, by electropolymerization, onto the transducer surface. Then, the oxytocin template was removed under potentiostatic conditions in a strong base solution.

Although the chemosensor detectability at the current stage of our research is insufficient to determine oxytocin at the nM level found in biological samples, the obtained results indicate suitability of the chemosensor for oxytocin determination in a μM range in a control serum sample. Moreover, the selectivity result of the chemosensor was quite promising. We achieved a very high selectivity over carbetocin, a peptide similar to oxytocin. In addition, the chemosensor was not responsive to smaller amino acids occurring in real samples at much higher concentrations than that of oxytocin.

Acknowledgments

We thank Dr. Tiziana Benincori (Department of Chemical and Environmental Sciences, University of Insubria, Como, Italy) for synthesizing the cross-linking monomer, **CM**. The present research was financially supported by Ministry of Science and Higher Education of Poland (grant no. IP2014 041473 to P.S.S.). W.K. and K.N. acknowledge National Science Center of Poland, NCN (Grant NCN No. 2014/15/B/NZ7/01011 and 2014/15/B/ST4/04642, respectively) for financial support. Z.I. acknowledges Ministry of Science and Higher Education of Poland (grant no. IP2014 041473) for financial support. FD is thankful to the National Science Foundation (grant no. 1401188) for financial support.

References

Anderson, G.M., 2015. Autism biomarkers: Challenges, pitfalls and possibilities. J. Autism Dev. Disord. 45, 1103-1113.

Birnbaumer, G.M., Lieberzeit, P.A., Richter, L., Schirhagl, R., Milnera, M., Dickert, F.L., Bailey, A., Ertl, P., 2009. Detection of viruses with molecularly imprinted polymers integrated on a microfluidic biochip using contact-less dielectric microsensors. Lab Chip 9, 3549-3556.

Channon, R.B., Joseph, M.B., Macpherson, J.V., 2016. Additive manufacturing for electrochemical (micro)fluidic platform. Electrochem. Soc. Inter. 25, 63-68.

Cheng, Z., Wang, E., Yang, X., 2001. Capacitive detection of glucose using molecularly imprinted polymers. Biosens. Bioelectron. 16 179-185.

Ertürk, G., Berillo, D., Hedström, M., Mattiasson, B., 2014. Microcontact-BSA imprinted capacitive biosensor for real-time, sensitive and selective detection of BSA. Biotechnol. Rep. 3 65-72.

Ertürk, G., Hedström, M., Mattiasson, B., 2016. A sensitive and real-time assay of trypsin by using molecular imprinting-based capacitive biosensor. Biosens. Bioelectron. 86 557-565.

Ertürk, G., Mattiasson, B., 2017. Capacitive biosensors and molecularly imprinted electrodes. Sensors 17, 390.

Frisch, M.J., *et. al.* 2009. Gaussian 09, Gaussian, Inc. Wallington CT.

Frustaci, A., Neri, M., Cesario, A., B.Adams, J., Domenici, E., Bernardina, B.D., Bonassi, S., 2012. Oxidative stress-related biomarkers in autism: Systematic review and meta-analyses. Free Radic. Biol. Med. 52, 2128-2141.

Graniczkowska, K., Pütz, M., Hauser, F.M., Saeger, S.D., Beloglazova, N.V., 2017. Capacitive sensing of N-formylamphetamine based on immobilized molecular imprinted polymers. Biosens. Bioelectron 92, 741-747.

Green, L., Fein, D., Modahl, C., Feinstein, C., Waterhouse, L., Morris, M., 2001. Oxytocin and autistic disorder: Alterations in peptide forms. Biol. Psychiatry 50, 609-613.

Haupt, K., Mosbach, K., 1998. Plastic antibodies: developments and applications. Trends Biotechnol. 16, 468-475.

Heinze, J., Frontana-Uribe, B.A., Ludwigs, S., 2010. Electrochemistry of conducting polymerss persistent models and new concepts. Chem. Rev. 110, 4724-4771.

Hong, C.-C., Chang, P.-H., Lin, C.-C., Hong, C.-L., 2010 A disposable microfluidic biochip with on-chip molecularly imprinted biosensors for optical detection of anesthetic propofol. Biosens. Bioelectron. 25, 2058-2064.

Huynh, T.-P., B.K.C., C., Sosnowska, M., W.Sobczak, J., Nesterov, V.N., D'Souza, F., Kutner, W., 2015a. Nicotine molecularly imprinted polymer: Synergy of coordination and hydrogen bonding. Biosens. Bioelectron. 64, 657-663.

Huynh, T.-P., Pietrzyk-Le, A., K.C., C.B., Noworyta, K.R., Sobczak, J.W., Sharma, P.S., D'Souza, F., Kutner, W., 2013. Electrochemically synthesized molecularly imprinted polymer of thiophene derivatives for flow-injection analysis determination of adenosine-5'-triphosphate (ATP). Biosens. Bioelectron. 41, 634-641.

Huynh, T.-P., Sharma, P.S., Sosnowska, M., D'Souza, F., Kutner, W., 2015b. Functionalized polythiophenes: Recognition materials for chemosensors and biosensors of superior sensitivity, selectivity, and detectability. Prog. Polym. Sci. 47, 1-25.

Jamróz, M.H., 2004-2010. Vibrational Energy Distribution Analysis VEDA, Spectroscopy and molecular modelling group, Institute of Nuclear Chemistry and Technology, Warsaw, Poland.

Jamróz, M.H., 2013. Vibrational energy distribution analysis (VEDA): Scopes and limitations. Spectrochim. Acta, Part A: Mol. Biomol. Spectr. 114, 220.

Jamróz, M.H., 2014. SPESCA, Spectroscopy and Molecular Modeling Group, Institute of Nuclear Chemistry and Technology; Warsaw, Poland.

Kukucka, M.A., Misra, H.P., 1994. Determination of oxytocin in biological samples by isocratic high-performance liquid chromatography with coulometric detection using C18 solid-phase extraction and polyclonal antibody-based immunoaffinity column purification. J. Chromatogr. B 653,, 139-145.

Lin, C.-C., Wang, G.-R., Liu, C.-Y., 2006. A novel monolithic column for capillary electrochromatographic separation of oligopeptides. Anal. Chim. Acta 572, 197-204.

Mabrouk, O.S., Kennedy, R.T., 2012. Simultaneous oxytocin and arg-vasopressin measurements in microdialysates using capillary liquid chromatography-mass spectrometry. J. Neurosci. Methods 209 127-133.

Madrigal, M.M.P., Giannotti, M.I., Oncins, G., Franco, L., Armelin, E., Puiggali, J., Sanz, F., Valle, L.J.d., Aleman, C., 2013. Bioactive nanomembranes of semiconductor polythiophene and thermoplastic polyurethane: thermal, nanostructural and nanomechanical properties. Polym. Chem. 4, 568-583.

Mermilliod, N., Tanguy, J., Petiot, F., 1986. A study of chemically synthesized polypyrrole as electrode material for battery applications. J. Electrochem. Soc. 133, 1073-1079.

Modahl, C., Green, L., Fein, D., Morris, M., Waterhouse, L., Feinstein, C., Levin, H., 1998. Plasma oxytocin levels in autistic children. Biol. Psychiatry 43, 270-277.

Orazem, M.E., Tribollet, B., 2008. Electrochemical impedance spectroscopy. John and Wiely, Hoboken, New Jursey.

Rachkov, A., Minoura, N., 2000. Recognition of oxytocin and oxytocin-related peptides in aqueous media using a molecularly imprinted polymer synthesized by the epitope approach. J. Chromatogr. A 889, 111-118.

Sannicolò, F., Mussini, P.R., Benincori, T., Martinazzo, R., Arnaboldi, S., Appoloni, G., Panigati, M., Procopio, E.Q., Marino, V., Cirilli, R., Kutner, W., Noworyta, K., Pietrzyk-Le, A., Iskierko, Z., Bartold, K., 2016. Inherently chiral spider-like oligothiophenes Chem. Eur. J. 22, 10839-10847.

Sharma, P.S., Dabrowski, M., D'Souza, F., Kutner, W., 2013. Surface development of molecularly imprinted polymer films to enhance sensing signals. TrAC-Trends Anal. Chem. 51, 146-157.

Sharma, P.S., Iskierko, Z., Pietrzyk-Le, A., D'Souza, F., Kutner, W., 2015. Bioinspired intelligent molecularly imprinted polymers for chemosensing: A mini review. Electrochem. Commun. 50, 81-87.

Sharma, P.S., Pietrzyk-Le, A., D'Souza, F., Kutner, W., 2012. Electrochemically synthesized polymers in molecular imprinting for chemical sensing. Anal. Bioanal. Chem. 402, 3177-3204.

Szeto, A., McCabe, P.M., Nation, D.A., Tabak, B.A., Rossetti, M.A., McCullough, M.E., Schneiderman, N., Mendez, A.J., 2011. Evaluation of enzyme immunoassay and radioimmunoassay methods for the measurement of plasma oxytocin. Psychosom Med. 73, 393-400.

Tamboli, V.K., Bhalla, N., Jolly, P., Bowen, C.R., Taylor, J.T., Bowen, J.L., Allender, C.J., Estrela, P., 2016. Hybrid synthetic receptors on MOSFET devices for detection of prostate specific antigen in human plasma. Anal. Chem. 88, 11486-11490.

Weng, C.-H., Yeh, W.-M., Ho, K.-C., Lee, G.-B., 2007. A microfluidic system utilizing molecularly imprinted polymer films for amperometric detection of morphine. Sens. Actuators B 121 576-582.

Woods, A.G., Wetie, A.G.N., Sokolowska, I., Russell, S., Ryan, J.P., Michel, T.M., Thome, J., Darie, C.C., 2013. Mass spectrometry as a tool for studying autism spectrum disorder. J. Mol. Psychiatry 1, 6.

Yates, K., Couteur, A.L., 2008. Diagnosing autism. Paediatric Child Health 19, 55-59.

Yola, M.L., Atar, N., Erdem, A., 2015. Oxytocin imprinted polymer based surface plasmon resonance sensorand its application to milk sample. Sens. Actuators, B 221 842-848.

Yoshimi, Y., Sato, K., Ohshima, M., Piletska, E., 2013. Application of the 'gate effect' of a molecularly imprinted polymer grafted on an electrode for the real-time sensing of heparin in blood. Analyst 138, 5121-5128.

Zhang, G., Zhang, Y., Fast, D.M., Lin, Z., Steenwyk, R., 2011. Ultra sensitive quantitation of endogenous oxytocin in rat and human plasma using a two-dimensional liquid chromatography–tandem mass spectrometry assay. Anal. Biochem. 416, 45-52.

Zheng, C., Liu, Z., Gao, R., Zhang, L., Zhang, Y., 2007. Recognition of oxytocin by capillary electrochromatography with monolithic tetrapeptide-imprinted polymer used as the stationary phase. Anal. Bioanal. Chem. 388, 1137-1145.

Figure Captions

Scheme 1. Optical camera photos of the Au thin-film electrode (diameter 1 mm) (a) after polymer film deposition, (b) zoomed image showing full coverage of the electrode surface, (c) the Au thin-film electrode assembling in the microfluidic system, and (d) the microfluidic system after complete assembling.

Scheme 2. (a) Structural formulas of functional monomers used to construct a molecular cavity for oxytocin in MIP, 4-bis(2,2'-bithien-5-yl)methylbenzoic acid glycol ester, **FM 1**; 1-methylamide-4-[bis(2,2'-bithienyl)methane, **FM 2**; bis(2,2'-bithienyl)-(4-(2-hydroxyethoxy)phenyl)methane, **FM 3**; (b) the amino acid sequence in the oxytocin analyte and the carbatocin interference.

Figure 1. High-resolution XPS spectra in the range of the nitrogen atom binding energy for the MIP film (*1*) before and after oxytocin template extraction under potentiostatic conditions at 0.50 V vs. Ag/AgCl with 0.01 mM NaOH for (*2*) 5, and (*3*) 8 h.

Figure 2. Atomic force microscopy (1×1 μm^2) images recorded using the semi-contact mode for the oxytocin imprinted polymer (a) before and (c) after extraction of the oxytocin template as well as for the non-imprinted polymer film (b) before and (d) after a treatment similar to that of the MIP film. The energy dissipation image of the oxytocin imprinted polymer (e) as prepared, and (g) after extraction of the oxytocin template as well as for the non-imprinted polymer film (f) as prepared and (h) after treatment similar as that of the MIP film.

Figure 3. The capacitance change with time after consecutive injections of 20-µL samples of oxytocin over the (a) oxytocin-templated MIP and (b) NIP film. (c) The capacitance change after consecutive injecting of carbetocin of different concentrations over oxytocin-templated MIP film. (d) The capacitance change with time after injection of 20-µL samples of oxytocin of different concentrations, indicated with numbers at curves, in NORTROL control serum, under FIA conditions for the oxytocin-templated MIP film. Insets show corresponding calibration plots. The 0.01 M KF solution was used as the carrier solution.

Table 1. Nanomechanical properties of MIP and NIP films.

Sample	DMT Young modulus, GPa	Deformation, nm	Adhesion, nN	Energy dissipation, keV
MIP				
as prepared	6.1 ± 2.2	8.5 ± 2.5	61 ± 9	0.9 ± 0.1
after template extraction	0.6 ± 0.2	6.8 ± 0.5	52 ± 9	19.2 ± 3.6
NIP				
as prepared	22.6 ± 2.3	5.8 ± 1.6	45 ± 2	0.8 ± 0.2
after treatment similar as that of MIP	10.9 ± 1.4	13.3 ± 1.5	91 ± 8	6.4 ± 1.9

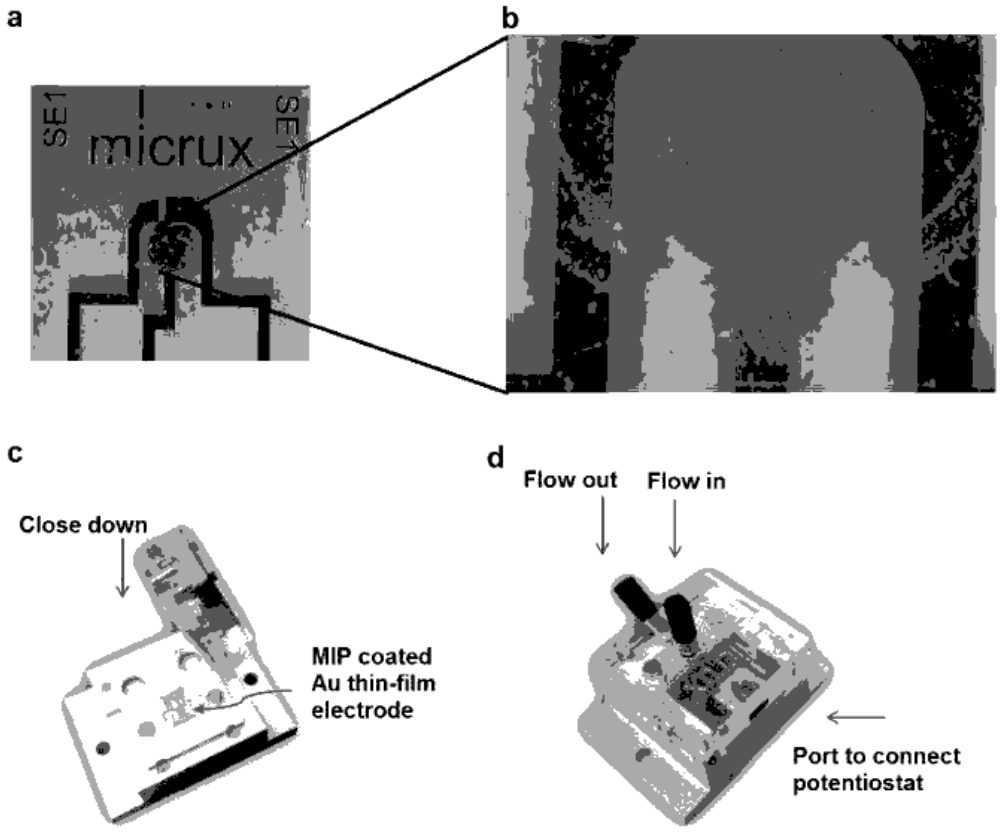
a
b
SE1
micrux
SE1
c
Close down
MIP coated
Au thin-film
electrode
d
Flow out
Flow in
Port to connect
potentiostat

Scheme 1

a

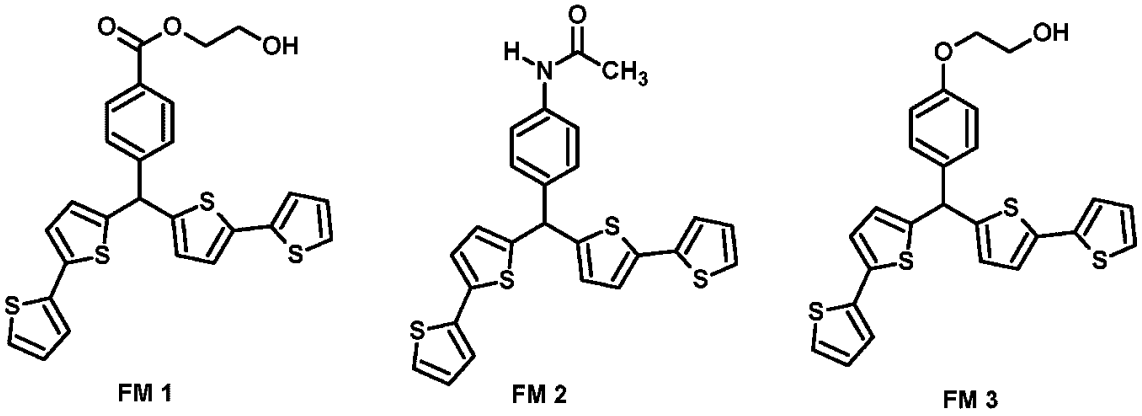
FM 1
FM 2
FM 3

b

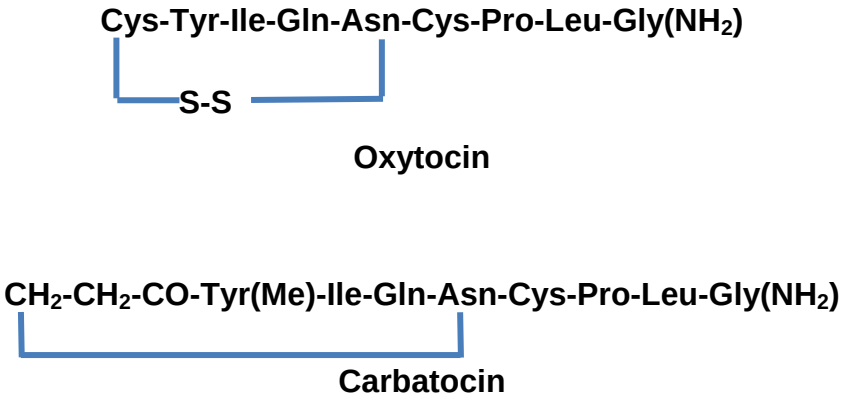
Cys-Tyr-Ile-Gln-Asn-Cys-Pro-Leu-Gly(NH2)
S-S
Oxytocin
CH2-CH2-CO-Tyr(Me)-Ile-Gln-Asn-Cys-Pro-Leu-Gly(NH2)
Carbatocin

Scheme 2

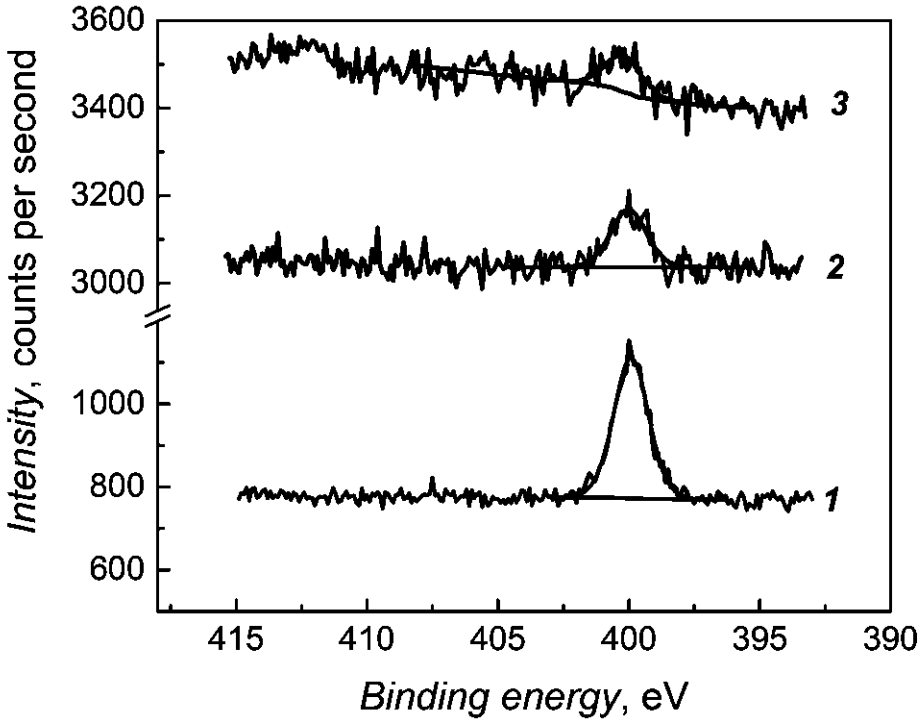
3600
3400
3200
3000
1000
800
600
Intensity, counts per second
415
410
405
400
395
390
Binding energy, eV
3
2
1

Figure 1

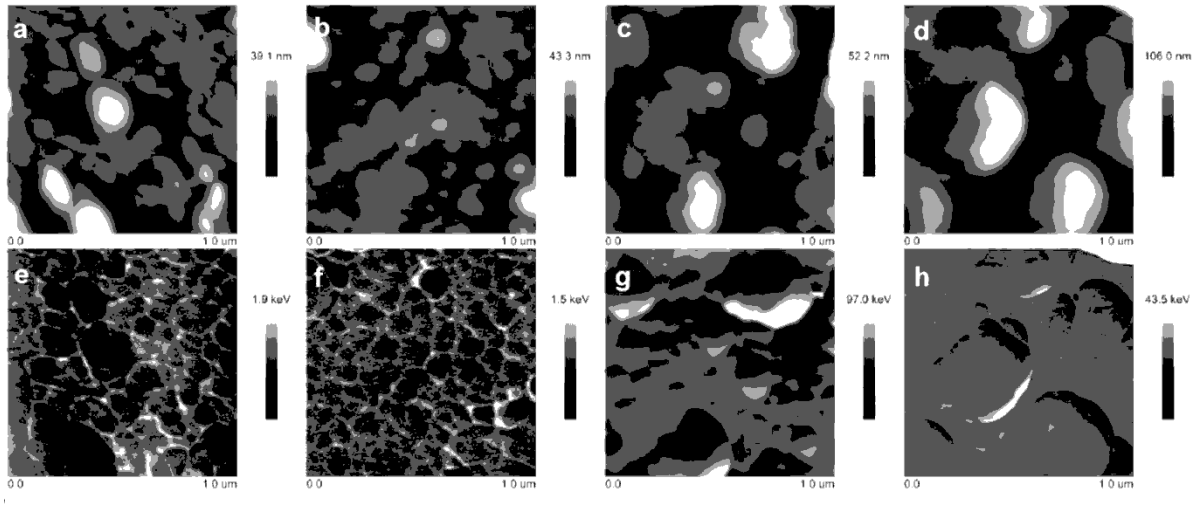
a
39.1 nm
0.0
1.0 um
b
43.3 nm
0.0
1.0 um
c
52.2 nm
0.0
1.0 um
d
106.0 nm
0.0
1.0 um
e
1.9 keV
0.0
1.0 um
f
1.5 keV
0.0
1.0 um
g
97.0 keV
0.0
1.0 um
h
43.5 keV
0.0
1.0 um

Figure 2

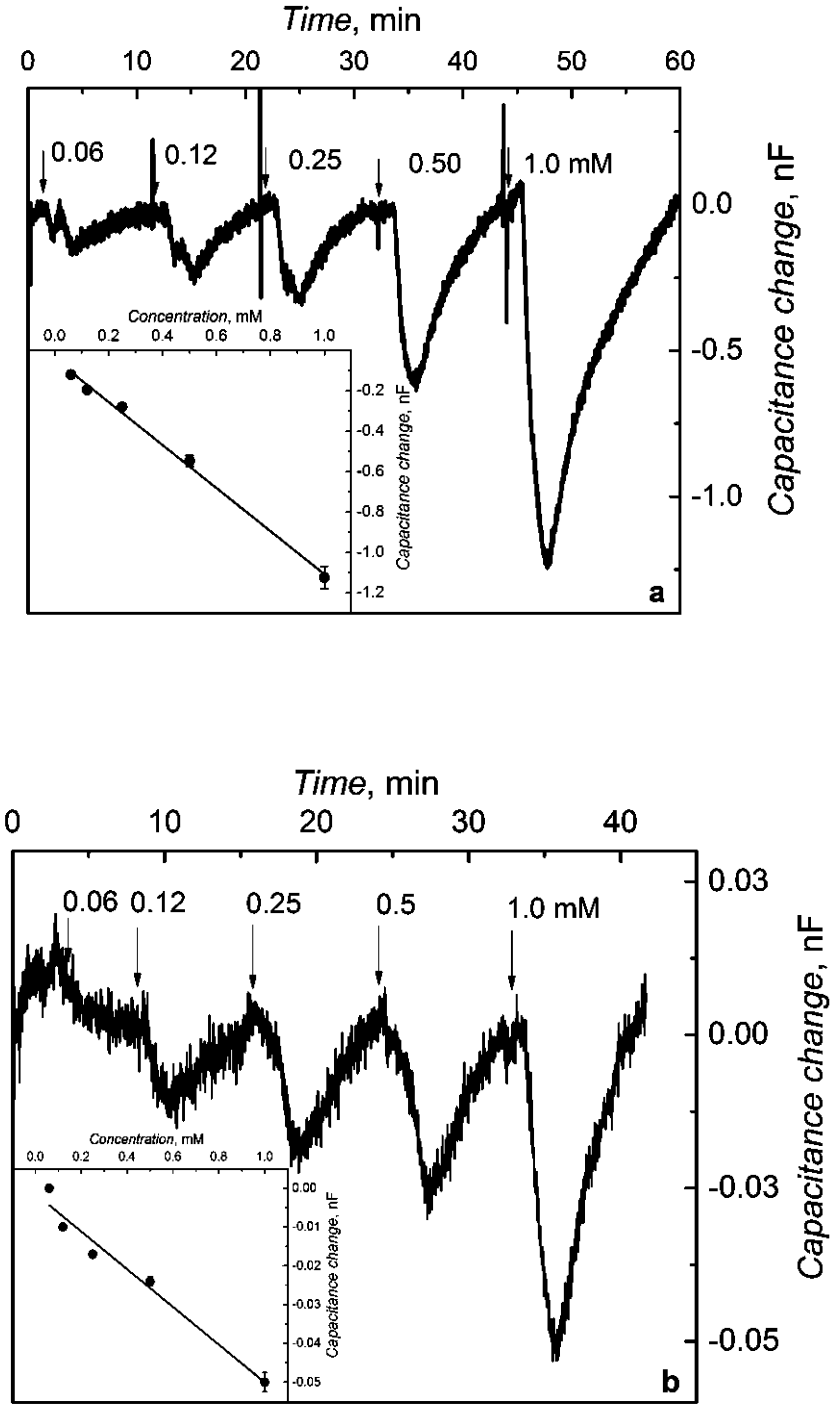
Time, min
0
10
20
30
40
50
60
0.06
0.12
0.25
0.50
1.0 mM
0.0
-0.5
-1.0
Capacitance change, nF
Concentration, mM
0.0
0.2
0.4
0.6
0.8
1.0
-0.2
-0.4
-0.6
-0.8
-1.0
-1.2
Capacitance change, nF
a
Time, min
0
10
20
30
40
0.06
0.12
0.25
0.5
1.0 mM
0.03
0.00
-0.03
-0.05
Capacitance change, nF
Concentration, mM
0.0
0.2
0.4
0.6
0.8
1.0
0.00
-0.01
-0.02
-0.03
-0.04
-0.05
Capacitance change, nF
b

Figure 3 (a, b)

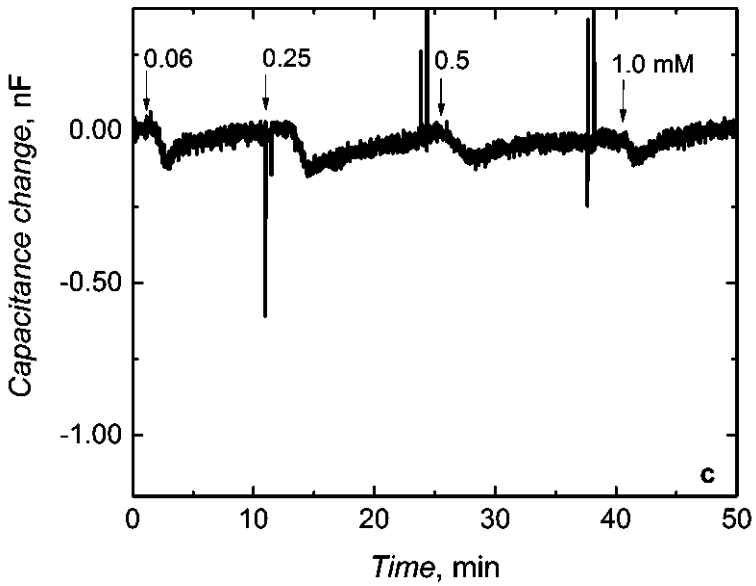
0.06
0.25
0.5
1.0 mM
0.00
-0.50
-1.00
Capacitance change, nF
c
0
10
20
30
40
50
Time, min

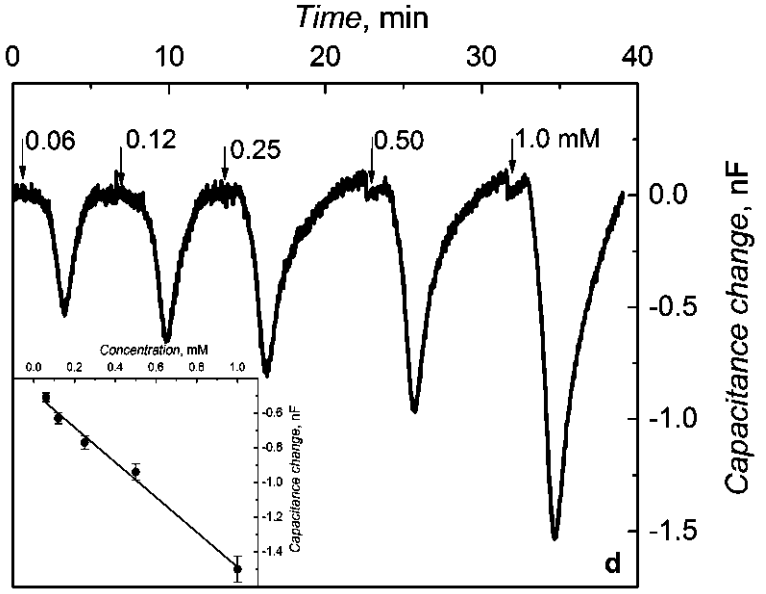
Time, min
0
10
20
30
40
0.06
0.12
0.25
0.50
1.0 mM
0.0
-0.5
-1.0
-1.5
Capacitance change, nF
Concentration, mM
0.0
0.2
0.4
0.6
0.8
1.0
-0.6
-0.8
-1.0
-1.2
-1.4
Capacitance change, nF
d

Figure 3 (c, d)

Highlights

- By means of molecular imprinting, we design molecular cavities selective for oxytocin nonapeptide,
- Suitable functional monomers were selected by computational modeling.
- We successfully combined a microfluidic platform, molecular imprinting, and electrochemical transduction.
- A miniaturized chemosensor for oxytocin determination in biological sample was devised.